ADVANCED ENGINEERING MATERIALS

DOI: 10.1002/adem.201600544

Thermal Cycling Behavior of Thin WC-Co Sintered Pellets**

By *Esteben A. Álvarez, José Luis García* and *Carlos J. R. González Oliver**

Hexagonal WC crystal phase, with a and c axis slightly larger than expected is obtained for thin sintered (at 1 400 ºC under vacuum) WC-20wt% Co samples having no extra carbon added. This effect can be associated with the elastoplastic hysteretic thermal expansion behavior detected in the thin disks and to the associated observed anisotropy showing a higher expansivity in the axial compared to the in-plane direction. By using a two phase model where the matrix is WC and the second phase is Co, it can be computed (from expansion data) that tensile forces are acting at room temperature in both directions for the examined specimen. By heating to about 50–80 ºC the strains/stresses become compressive as expected for WC-20wt% Co.

There is strong interest to produce fine grained WC/Co[1–5] composites and related metal matrix composites (MMC), including those made through chemical synthesis, of acceptable toughness and hardness,[6–9] as well as to determine precisely the densification and grain growth kinetics involved in such typical systems.[10–17]

Crystalline phases formed in thin (≈1 mm) pellets of tungsten carbide compositions having large Co content (20 wt%) and having no extra C added are analyzed in this work. For these specimens slightly expanded a, *c*-axis of the WC unit cell were obtained. A previous work[18] considered densification kinetics analysis for WC + 2, 5, and 10% Co compositions (prepared in a similar way to the present 20 wt% Co samples). It is relevant to note that such specimens densified initially from 800 to about 1 200 °C by grain growth kinetics (solid state sintering) and that from 1 200 to 1 400 °C, the liquid phase sintering process was the main acting densification mechanism. Although, for the latter range also grain growth kinetics (in the presence of a liquid phase) and particle rearrangement in presence of liquid phase also contributed to the densification. Aiming at identifying the origin of such WC unit cell expansion, thermal expansion cycling data were collected up to 700–800 °C under vacuum. Measurements gave elastoplastic hysteretic thermal expansion behavior and different expansivities in the perpendicular direction as compared to the in-plane expansion of present pellets. A residual strain/stress spatial-distribution model is proposed to explain the cycling evolution.

[*] *Dr. C. J. R. González Oliver*
Centro Atómico Bariloche - CNEA, Av. E. Bustillo 9500, RA-8400 Bariloche, Argentina
E-mail: gon@cab.cnea.gov.ar
Dr. C. J. R. González Oliver, E. A. Álvarez
CONICET, Godoy Cruz 2290, C1425FQB, Buenos Aires, Argentina
Dr. J. L. García
Sandvik Coromant R&D, SE-12680 Stockholm, Sweden

[**] *The ANPCyT is acknowledged for financial support provided by project PICT2010-1759 and are thanked Mr. M. Sanfilippo (MaterialesNucleares, CAB), and Miss Paula Troyon (Caracterización de Materiales, CAB) for important technical support and help during the present work. Dr. Alejandra Montenegro is thanked for performing the Rietveld analysis. We are also indebted to Universidad National de Cuyo, project 06/C372, CONICET project PIP1122011010053301, and the Joint European Master Programme on Advanced Materials Science and Engineering and FP7-IRSES Project Nr. 247524 "NanoCom Network".*

1. Experimental Section

The WC/Co compositions (Table 1) were obtained by mixing WC (Starck; grade 4NPO: specific surface area of 4 $m^2\ g^{-1}$) with fine Co particles (see Figure 1). They were prepared through mixing at 400 rpm for 20 h, using an aqueous-alcoholic mix of 46 g [52 wt% H_2O. 48% C_2H_5OH] containing about 2.5 g of 80 wt% WC and 20% Co powder (Merck, #12211, Germany). The mixture was dried in a rotoevaporator at 80 °C under vacuum. The pellets for sintering were prepared by adding to the previous powder 2 wt% PVB (MW 150000, polyvinyl butyral, Polyscience Inc./USA) and pressed uniaxially in a steel mould ($\phi_i = 6.08$ mm) at approximately 243.2 MPa for 2 min. Therefore, every specimen for sintering in the vacuum furnace was in the form of

Table 1. Chemical compositions (wt%) examined.

Code	WC	Co [wt%]	Al_2O_3 relative to WC + Co
Mx; M1, M2, M3, M5, M6, M7	80	20	
M8; cycled specimens: 1st heating in-plane (M8a), 2nd heating perpendicular (M8b), 3rd heating in-plane (M8c)	80	20	
MxA; M1A, M2A, M3A, M5A, M6A	79.43	19.86	0.7%

Table 2. Heat treatment schedules with the detailed associated specimens.

Codes	Initial heating [IT] step [10%H_2-Ar]	Final heat treatment step [vacuum 0.07 mbar]	
HT1 (compositions M1, M1A)	RT–560 °C 3 °C min^{-1}	560–1 360 °C 3 °C min^{-1}	4 h
HT2 (M2, M2A)	RT–560 °C 3 °C min^{-1}	560–1 360 °C 3 °C min^{-1}	2 h
HT3 (M3, M3A)	20–645 °C 3 °C min^{-1}	645–1 364°C 3 °C min^{-1}	2 h
HT5 (M5, M5A)	RT–600 3 °C min^{-1}	600–1 350 °C 3 °C min^{-1}	2 h
HT6 (M6, M6A)	RT–800 3 °C min^{-1}	800–1 350 °C 3 °C min^{-1}	2 h
HT7 (M7)	RT–600 °C 3 °C min^{-1}	600–1 360 °C 3 min^{-1}	6 h
HT8 (M8; sample used for thermal expansion cyclings)	RT–800 °C 7 °C min^{-1}	800–	2 h
HT8a, 1st heating of M8 in-plane direction; (M8a)	5 °C min^{-1}	RT–850 °C	
HT8b, 2nd heating (of M8 + HT8a) in perpendicular direction; (M8b)	5 °C min^{-1}	RT–850 °C	
HT8c, 3rd heating (of M8 + HT8a + HT8b) in plane direction; (M8c)	5 °C min^{-1}	RT–700 °C	
HTC, dilatometer-cyclings of commercial composition (CTI)	4–6 °C min^{-1}	RT–1 150 °C	

small disks of about 6 mm in diameter and thickness between 0.7 and 1.2 mm.

The specimens codes (see Tables 1 and 2) are Mx ($x = 1,2,..8$) and MxA ($x = 1,2,..8$), where the first series correspond to WC + Co only and the last one apply to WC + Co + Al_2O_3. Alumina was Aeroxide (Aluminiumoxid C) from the late Degussa-Hüls, Germany. The WC/20% Co specimens had "no extra carbon added" and the amount of colloidal alumina added was 0.7 wt% of the (WC + Co); thus a typical mixture contained 2 g WC, 0.5 g Co, and 0.0175 g Al_2O_3. These samples were sintered by heating up to approximately 600–800 °C under a flux of 10% H_2–Ar, and then further heated in vacuum (2.7–5.3 Pa) up to 1 360–1 400 °C (Table 2).

A vertical differential dilatometer (Dilatronic, Theta Inc., USA) was used to study the thermal expansion behavior of previously sintered pellets. The dilatometric curves represents (l(t, T)-lo)/lo as a function of temperature "T(°C)", where "l" is the instantaneous length (pellet height) and "lo" is the initial thickness. The thermal expansion of a particular pellet (M8x; WC–20 wt% Co, HT8) was measured, under vacuum, in in-plane direction by placing vertically the pellet inside a slot cut in a short (about 5 mm height) Al_2O_3 tube or silica tube, and calibrated with a similar disk made of high purity optical fiber-grade silica glass. The axial (1 mm height) expansion was measured (and calibrated with a similar thickness of such silica glass) by placing the flat pellet disk between zirconia thin disks. The sensing alumina rod (and extra weights) exerted a total charge/weight of about 6–8 g on the specimen. Regarding these vertical dilatometer data, it is important to note that this complex apparatus (consisting of several elements, such as alumina rods, weights, gas inlets/outlets, isolating thin ceramic pieces to avoid sticking of the sample to the alumina sensing rod among others) requires an important/careful set up, besides an appropriate sample preparation. In this case, the pellets exposed to heat treatments in the dilatometer were prepared and set up to avoid possible frictions or slippages inside the alumina tube during the measurements. However, a minimum wedge-shaped in the pellets could affect the obtained signals. This is the reason why the system configuration is very time consuming and demands a great effort to achieve repetitive measurements.

The XRD patterns were made using Philips PW1700 and PANAlytical Empyrean diffractometers. As the specimens were very hard after the sintering heat treatment, they were examined in plate form, such as the sample was stuck on a piece of glass and aligned parallel to the diffractometer reference planar surface. The diffraction patterns were X-pert analyzed and silicon spread onto the samples was used to calibrate the 2θ-angle in the diffraction patterns. For the SEM and microhardness observations and analysis a Phillips SEM515, SEM FEI Nova Nano SEM 230, FEI Helios 600, and Mitutoyo MVK-H0 were used. The specimens were machined with a diamond saw and polished manually using diamond impregnated polymer films (South Bay Technology, USA).

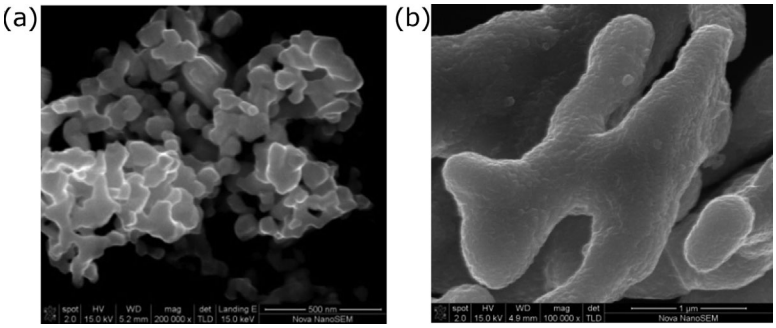

Fig. 1. (a) WC Starck powder, (b) Cobalt grains.

ADVANCED ENGINEERING MATERIALS **2017**,
DOI: 10.1002/adem.201600544

ADVANCED ENGINEERING MATERIALS

The heat treatment (HT)/sintering cycles (Table 2) were carried out in a SiC furnace fitted with an alumina tube having sealed inlet/outlets for gas atmospheres and where reasonable double-stage-pump (Edwards 5 Two Stage E2 M5) vacuum could be reached (1.3–40 Pa); Varian, 801, tc vacuum gauge).[11] The primary gas mixture (H_2/Ar) employed was 10% H_2–Argon 5.0 (Linde gas, $H_2O < 2.0$, $O_2 < 2.0$, $N_2 < 5.0$, $H_2 < 1.0$, $CH_4 < 1.0$, $CO < 1.0$ ppm/volume). Most of the HT cycles covered an initial heating (IT), at 3–5 °C min^{-1} heating rate, under a flow of the previous (H_2/Ar) up to about 600–800 °C, depending on composition, and then, the HT was continued at a similar rate up to generally 1 360 °C under maximum vacuum (2.7–6.7 Pa) achieved for the particular samples and HT. The specimens were placed over a high purity graphite plate (GP) inside an alumina boat, and they were covered with another GP.

2. Results

2.1. Microstructure of Sintered Specimens

In this section, the grain size distribution as well as the grain shape morphology obtained after the present two-stage heat treatment (Figure 2) are addressed. Macro physical properties, like microhardness and absolute thermal expansion coefficients, for specimens containing 20 wt% Co are reported and compared to the known literature values for specimens generally made under high vacuum or under oxygen-free inert gas flow conditions as exercised in industry.[1,8,13,21,22,27]

Regarding the initial heating step (IT), as well as the time at the final temperature of HT samples M5 (HT5) and M6 (HT6) are first considered, which differed mainly in the (IT) temperature, at which they were exposed to the gas flow (10% H_2/Ar) up to 600 (M5, HT5), and 800 °C (M6, HT6), respectively. In M5, an important proportion of Co_3W_3C was detected contrasting the situation for M6, for which only Co and WC are obtained (see Figure 3a and c). The number and size of the polycrystalline grains markedly differed in both specimens (see Figure 2a and b). By counting the number of WC grains cut by different random straight lines made in Figure 2a and b average WC grain-sizes of 1.3 and 1.6 μm can be estimated for specimens M5 and M6. This could imply that M6 has bigger grains, but a simple look at both figures indicates that M6 "has in fact a higher fraction of the smaller grains". M5 and M6 were compared to estimate, which one has the smaller grain size. Two regions (integrated by the smaller grains) of the same area were selected

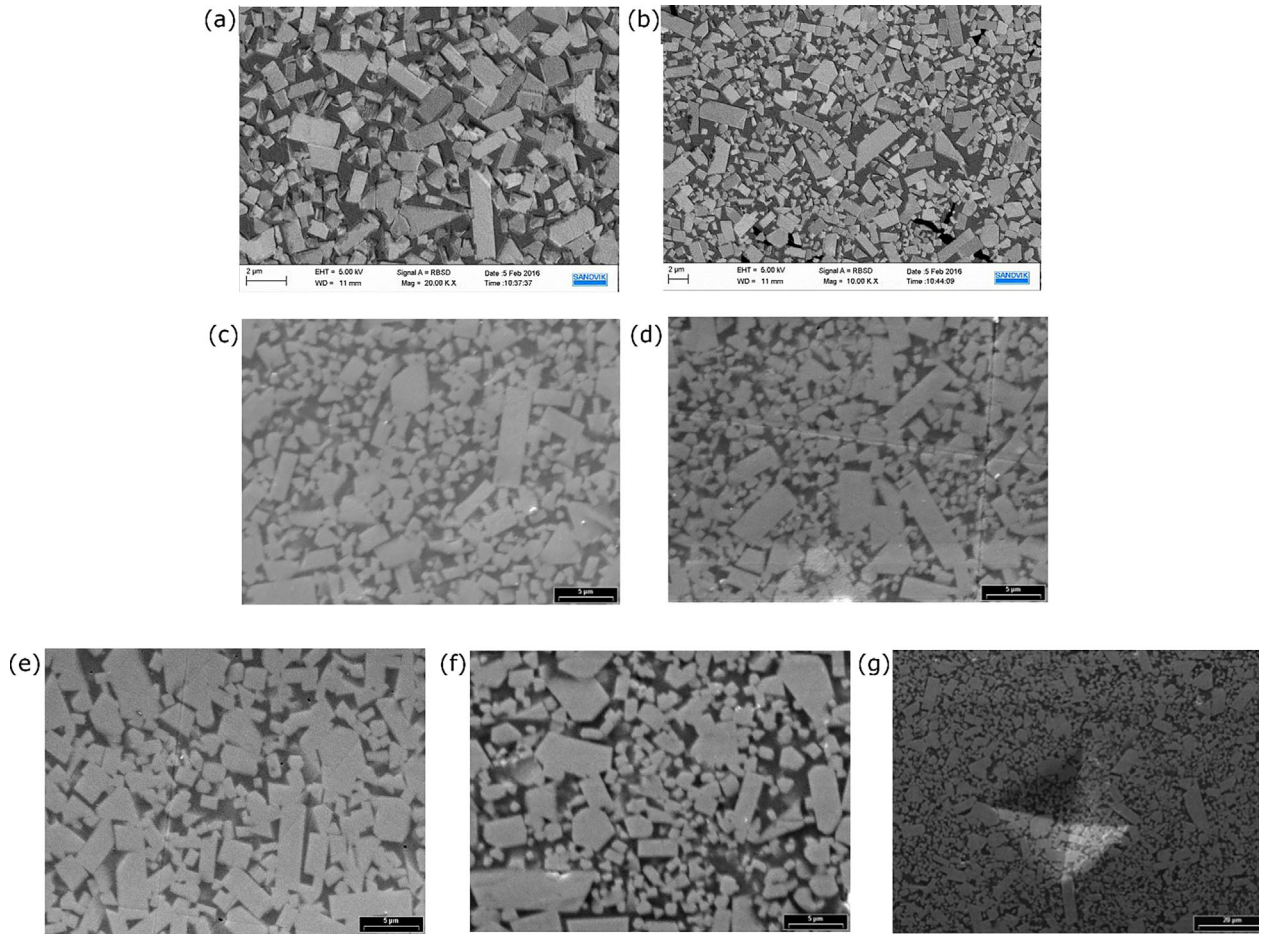

Fig. 2. (a) M5, (IT:600 °C), 1 354 °C (2 h), (b) M6, (IT:800 °C), 1 354 °C (2 h), (c) M3, HT3 (2 h), (d) M3A, HT3 (2 h), (e) M1, HT1 (4 h), (f) M7, HT7 (6 h), and (g) M7, HT7 (6 h).

DOI: 10.1002/adem.201600544

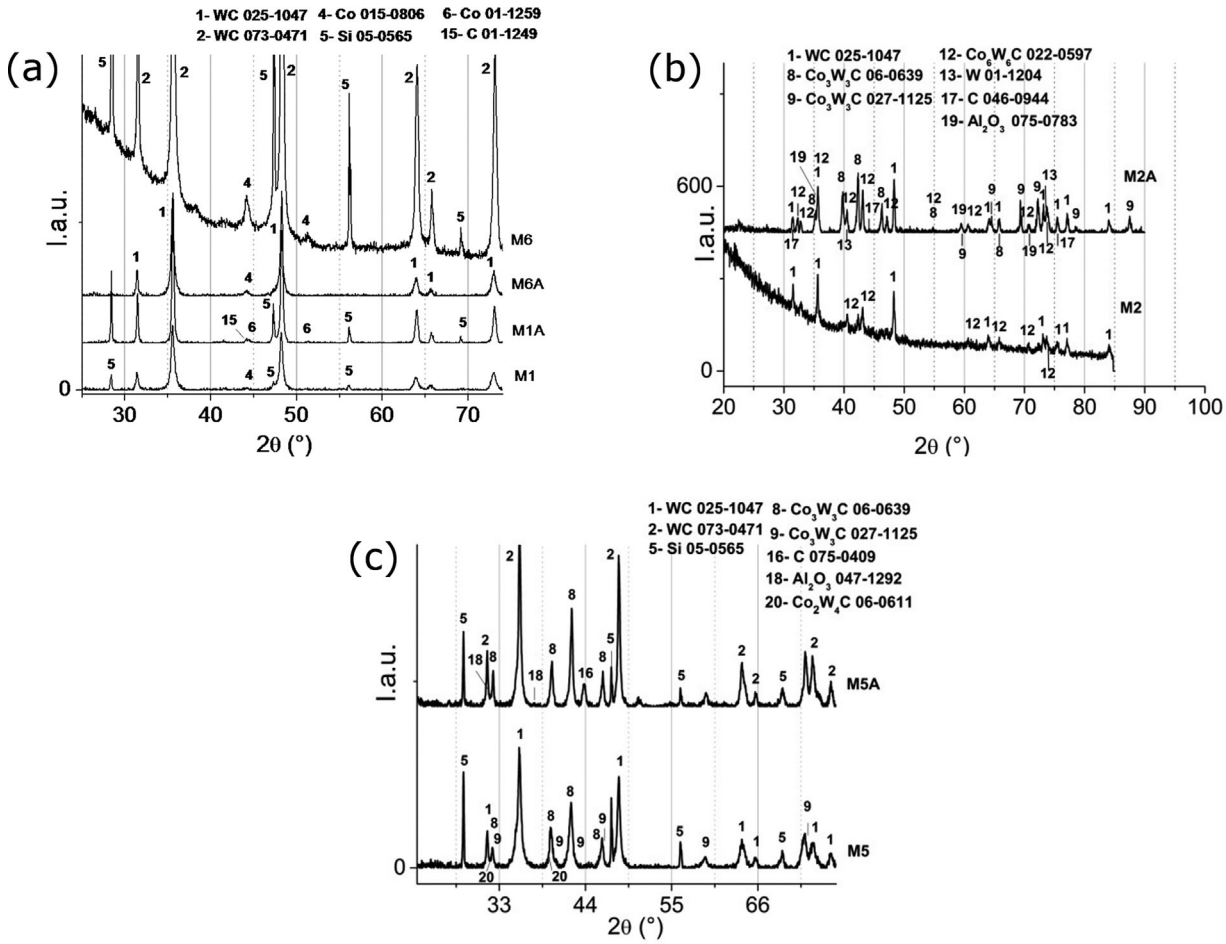

Fig. 3. XRD patterns of simultaneously sintered compositions (a) M1, M1A (HT1) and M6, M6A (HT6), (b) M2, M2A (HT2), and (c) M5, M5A (HT5).

to estimate the number of particles per unit area and the number of particles per unit volume (N_v). The area of the analyzed regions was 41 μm^2. N_v was roughly estimated as N_A/D, where N_A is the number of particles per unit area and D corresponds to the larger grain-size in that population. For M5 (35 grains in an area of $41 \times 10^{-12}\,m^2$) and M6 (56 grains inside $41 \times 10^{-12}\,m^2$) N_A/D were, respectively, (0.85 μm^{-2}/1.89 μm) 0.45×10^{18} and (1.37 μm^{-2}/2 μm) 0.68×10^{18} particles per unit volume (m^{-3}). The larger N_v for M6 ($\approx 1.5 N_{V(M5)}$) implies that this sample has the highest number of WC-grains per unit volume of material in the fine particle-regions remarking the strong effect of the (IT) up to which the mix (H_2/Ar) was flowing during the heat treatment.

In Figure 2c and e–g, micrographs for specimens Mx (similarly pressed and without alumina additions) after heatings at 1 364 °C for 2 [M3, HT3, (IT: 645 °C), 1 364 °C], 4 [M1, HT1, (IT: 558 °C), 1 364 °C] and 6 h [M7, HT7, (IT: 600 °C), 1 364 °C] are shown. Quite different microstructures are observed. From 2 to 4 h at 1 354 °C, the average grain size increases, decreasing the total number of grains. From 4 to 6 h, an important proportion of WC-grains decomposed into smaller ones and it is also detected an increase in the size of the largest particles.

The effect of alumina additions to WC/Co compositions can be noted in Figure 2c and d. Although, there is a greater proportion of smaller grains in M3A (HT3, 2 h), nearly no change in the size of the largest grains for this specimen M3A (HT3) compared to M3 (HT3) can be detected.

Regarding the Vickers Hardness in Figure 2g, an indentation obtained in specimen M7 (HT7), using the equipment Mitutoyo MVK-H0 with a load of 500 g during 30 s is shown. The diagonal of the indentation has an average length of 41 μm (measured with JImage program;[19]). The Vickers microhardnesses for M2 and M7 samples were 1 017 and 1 242 HV. For these WC/Co compositions, these hardness values are clearly on the lower side of the expected microhardness and are assigned to the high Co-content (20 wt%) and to the remaining porosity, on average, of roughly 4% for the present specimens.

2.2. Crystal Phases Formed in These WC/Co Specimens

XRD patterns for M1and M6, to which no extra carbon was added during preparation are shown in Figure 3a. For every specimen after 1 362 °C, only WC and Co reflections are obtained. The intensity of the Co-peak is surprisingly too low, considering the nominal 20 wt% Co level. As the patterns for

ADVANCED ENGINEERING MATERIALS 2017,
DOI: 10.1002/adem.201600544

ADVANCED ENGINEERING MATERIALS

M1 and M6 were calibrated with the silicon reflections (as mentioned before, silicon was spread onto the samples to calibrate the 2θ-angle in the diffraction patterns), it is possible to estimate the values of the *a*- and *c*- axis of the hexagonal WC phase,[20] which for M1 and M6 are, respectively, 0.2912 (versus 0.29062) and 0.2847 nm (versus 0.28378; WC 025–1 047), and 0.2915 (versus 0.29064) and 0.2844 nm (versus 0.28369; WC 073–0471). As noted in refs.,[21–23,27] the relative expansion coefficients for *a*- and *c*-axis appear to depend on the specimen type and some changes in crystal morphology can also be expected due to the sintering temperature and the action of the liquid phase.

Specimen M6A was also examined in a high precision diffractometer (PANAlytical Empyrean) at a low scan speed of 0.154 (°) s^{-1} to produce a set of diffraction data suitable for Rietveld analysis. By this method, the previous expansions in *a*- and *c*- axis was confirmed. The values of *a*- and *c*-lattice parameters were estimated to be $a = 0.2911$ and $c = 0.2842$ nm. These are (M6A) slightly larger than the theoretical ones for a crystal WC: $a = 0.2906$ nm *y* $c = 0.2837$ nm.

In Figure 3a, the patterns of both specimens doped with alumina and heat treated differently: (M1A, M6A) are shown and compared to the previous M1 (HT1) having no alumina added. Again a similar situation as before concerning the expansion of the WC structure is obtained.

Sample M5 (Figure 3c) was heated up to IT = 600 °C under (H_2/Ar) and showed three subcarbide phases: Co_3W_3C (06–0639, Co_3W_3C (027–1 125) and CoW_4C (06–0611) and exhibited no Co-peaks. Similar situation was observed for M2 (Figure 3b) and for the companion compositions having ultrafine alumina added, M2A and M5A. The reason for this apparent WC decomposition generating W and C (for forming these subcarbides) with the nominal 20% Co (after the final 1 362 °C under vacuum) is still unclear, but it could be related to variations of flow rate of the initial 10% H_2-Ar mixtures meaning different quantities of oxygen impurities being present at the moment the medium (≈4 Pa) vacuum stage was activated and subsequently maintained up to about 1 400 °C. Even though, from direct comparison of peak intensities, it would appear that compositions with alumina decomposed a bit more into some subcarbides than for specimens without alumina. Furthermore, both specimens M5/M5A gave slightly expanded elementary *a*, *c* − axis of the WC phase.

The three specimens were dense with approximate densities of near 14 g cm^{-3} (see Figure 2) and with high hardness requiring diamond machining and polishing. The remaining porosity grossly ranged from 2 to 10% in these sintered specimens.

XRD patterns corresponding to the surfaces of M1 (separate furnace) and M8 (made in separate furnace and further cycled in the dilatometer) are shown in Figure 4, for as-made samples and after surface polishing, to detect possible gradients in chemical composition. WC and calibrating Si phases are shown by their corresponding peaks. The as-made surfaces of the samples were initially analyzed (M1, M8), and some of them were further thickness-reduced by gentle cutting using a low speed diamond disk, removing up to 50 micrometers material from each sample

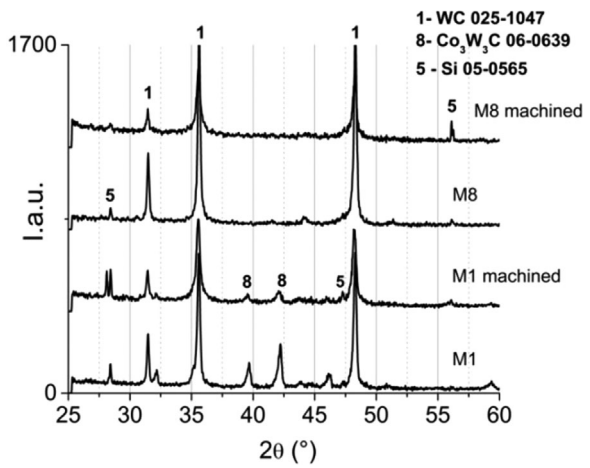

Fig. 4. XRD patterns of differently made samples.

(M1 machined, M8 machined). After manual polishing (using diamond impregnated films), the four samples were calibrated with silicon by using a Si-alcohol mixture ultrasonically dispersed, which was poured on the samples to calibrate 2θ diffraction angle in the XRD patterns. After the estimation of *a*- and *c*- axis of the hexagonal WC phase, again "expanded" WC structures were obtained. It is remarked that machined M8 (XRD examination of bulk M8) gave clearly expanded WC unit cell; M8 was the selected sample for the thermal expansion cycling and estimations of residual/internal strains/stresses.

2.3. Bulk Thermal Expansion Cyclings and Differential Strains in a Sintered Pellet Having 20 wt% Co

The dilatometric curves in Figure 5a show the thermal expansion curves of a 20 wt% Co disk-sample (M8), initially following the in-plane orientation (M8a), second along the perpendicular direction (M8b), and third according to the in-plane direction (M8c). The heating was up to 850 °C under vacuum for the first two orientations and up to 700 °C for the last one; the heating rate was 5 °C min^{-1} (see Table 2). These expansion curves recover the initial value after the heating/cooling cycles meaning a reproducible hysteretic behavior, which, in turn, can be associated to the smaller expansion of WC as compared to that for Co. It should be noted M8a and M8b corresponds to measurements using an alumina support and are related, respectively, to measurements following in-plane and perpendicular directions of the same pellet.

On the other hand, trace M8c corresponds to the third heating (in-plane direction) of the specimen, but using a silica glass tube-support. In relation to M8a and M8b, it is seen in Figure 5b that the pellet-specimen "expands more" in the perpendicular direction than in the longitudinal one. Also, at this stage, it is not clear whether the WC-matrix is under tensile stresses as it can be suggested by the XRD data in Figure 3a giving WC hexagonal structure with expanded *a*, *c*-axis. The lower curve (circular symbols; M8a) corresponds to the in-plane direction, whereas the upper curve applies to the perpendicular direction (square symbols; M8b).

DOI: 10.1002/adem.201600544

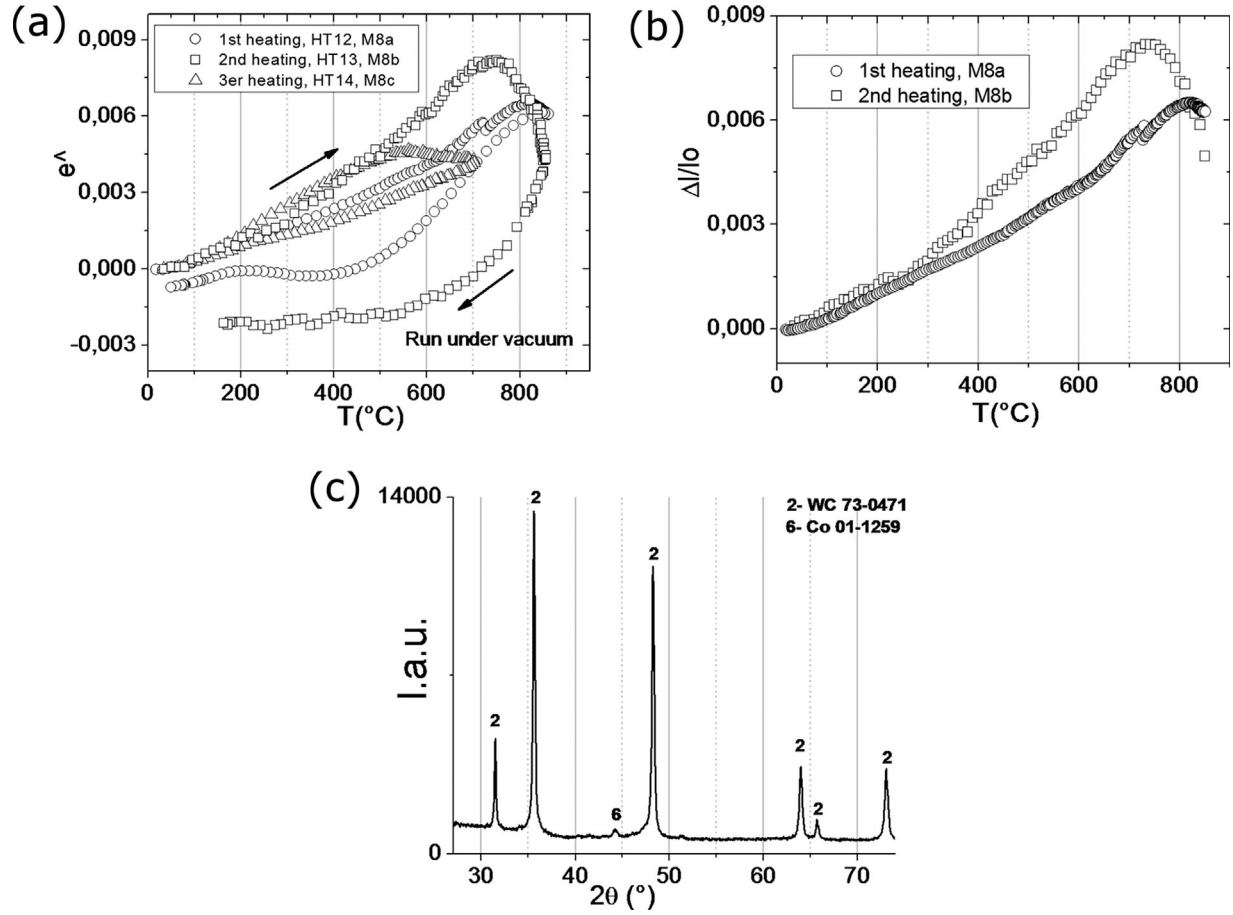

Fig. 5. (a) Absolute strain e^ (T) for specimen M8 under different orientations, (b) Thermal expansion of in-plane (circular symbols; M8a) and perpendicular (square symbols; M8b) directions of the sintered pellet M8, and (c) XRD of the specimen M8 after the 3rd heating (M8c).

During the heating (see M8a-trace in Figure 5a and b), a slight expansion is detected in the 150–600 °C range, giving an expansion of 75.5×10^{-7} ($°C^{-1}$). Then, from 600 up to 815 °C, the expansion increases, to a higher value of 119×10^{-7} ($°C^{-1}$). After the 3rd heating, the specimen did not exhibit any change in crystal structure respect to the initial condition, as shown in Figure 5c.

In Figure 6a the e^(T)-relative expansion data (M8c) obtained with a silica tube instead of the alumina tube after heating up to only 700 °C is shown. It had an apparent thermal expansion coefficient of 75×10^{-7}($°C^{-1}$) in the 500–200 °C cooling range, very similar to the one measured using the alumina tube (M8a). In Figure 6a, it has been tentatively plotted a line e^*(T) corresponding to a slope of about 81.5×10^{-7} (1/ °C), for a 20 wt% Co–80% WC (30.7% v/v Co. 69.3% WC) composition. This expansion was estimated from the rule of mixtures $\alpha_C = \alpha_{WC} V_{WC} + \alpha_{Co} V_{Co}$ [where the volume fractions $V_{WC} + V_{Co} = V_{WC} + (1 - V_{WC}) = 1$] using $V_{WC} = 0.693$, $V_{Co} = 0.307$, $\alpha_{WC} = 60 \times 10^{-7}$ ($°C^{-1}$) and $\alpha_{Co} = 130 \times 10^{-7}$ ($°C^{-1}$), and, WC and Co densities of 15.6 and 8.9 gcm^{-3}, respectively. In this rule of mixtures, contiguity factors (a measure of the contact area between grains) has not been considered yet, neither the thermal expansion anisotropy of the WC phase. It is noted that residual stresses must be operating, in this sample, as the upper and lower curves (Figure 6a) differ considerably from the linear one 81.5×10^{-7}(1/°C), and the curves form a closed loop as expected for a specimen recovering its initial e^(T) value.[25–27] Preliminary and attempting to sort out the type of stresses (compressive/tensile) acting on the matrix (WC) and second phase (Co) in this composite, the following difference value: $e = e^{\wedge}(T) - e^*(T)$ is presented in Figure 6b. From Figure 6b it is noted that the WC grains (matrix) would be under the action of tensile stresses at RT. Therefore, this model can predict a residual tensile stress at room temperature over the WC phase, and, it is solely due to the measured hysteretic elastoplastic behavior for a given direction. This effect consisted on expanding the composite WC + Co as elements (WC and Co) connected in series, such as the overall expansion is lower than that for Co and greater than that for WC due to a good strain-transference between these elements. On further heating, a temperature ($T1$) is reached where no more strain transference occurs and the composite tend to expand at the Co phase rate. This is so until the Co phase (upon further heating) is soft enough ($T2 > T1$), so that no more expansion is added, and the composite reduces its expansion to WC values. On cooling, this is somehow reversed and for instance a new $T1^*$ lower than $T1$ is obtained, as it may be noted in Figure 6a and **7**a.

Supporting the above conclusion, similar couple of graphs for the first/initial heating of specimen M8 (M8a; in-plane direction) are shown in Figure 7.

DOI: 10.1002/adem.201600544

ADVANCED ENGINEERING MATERIALS

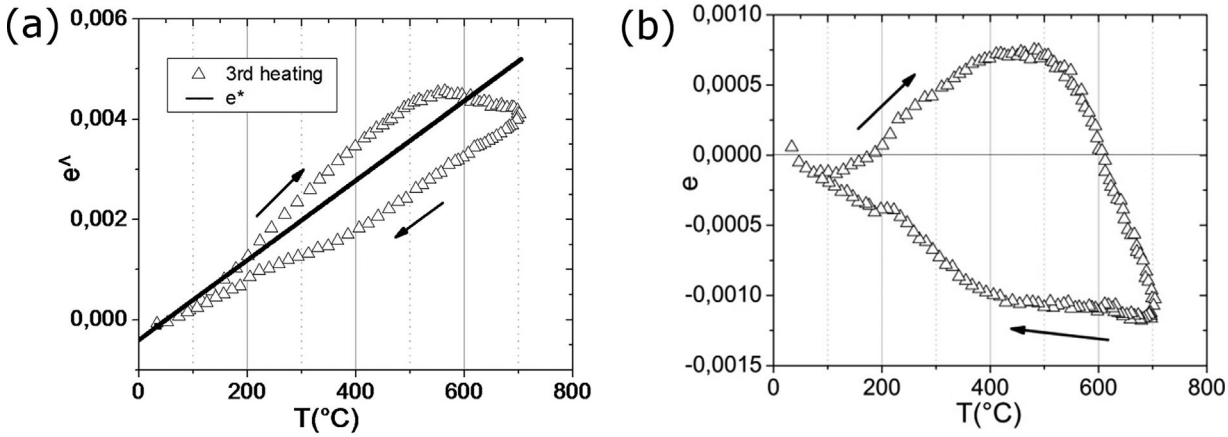

Fig. 6. (a) Expansion of specimen M8 after the 3rd heating (M8c); (b) Estimation of residual strains based on data in Figure 6a.

In Figure 7a, the straight line shown is the same as that in Figure 6a. Also, by comparing the 1st and 3rd cycles (see Figure 6b and 7b), some stress relaxation, of mainly the Co phase, takes place as indicated by the different extents covered in the upper and lower curves for the 1st and 3rd cycles.

Finally, it should be noted that a commercial WC-Co + TiC (CTI): cutting tool insert with unknown composition) was also measured in similar conditions for comparison purposes. The cycle curve is shown in Figure 8a together with that for the previous sample M8c.

The specimen CTI was not yet fully studied. A micrograph of the diamond polished CTI specimen is shown in Figure 8b. Three phases are detected i) white WC, ii) dark gray phase rich in TiC, and iii) black small zones rich in Co (and perhaps Nb). SEM–EDS point analysis collected for specimen CTI suggests that a small region containing a clear phase resulted in an elemental composition of 68.19% W, 11.33% C, 19.86% Co, and 0.62% Ti. The dark gray phase contains a large amount of Ti 13.02%, Nb 2.70%, 69.99% W, 13.18% C, and 1.12% Co approximately. The black small zones are still unresolved.

The thermal expansion hysteretic clear loop detected for CTI could be assigned to a similar biphasic behavior of carbides grains within a Co-rich metallic matrix, as reported above for M8 specimen.

The hysteretic loops are different for M8c and CTI, as well as the limiting expansivities. For M8c the initial thermal expansion is clearly larger than that for CTI, and this is attributed to a larger Co level (20 wt%) in M8c as compared to that for CTI. Also the "softening" temperatures of about 500 °C for M8c and 800 °C for CTI are markedly different. In CTI, it is possible that the solid phase is a mixture of WC and TiC phases and that the content of the metallic Co-rich phase is smaller than that for M8c.

3. Discussion

The H.C. Starck powder used in this work is considered of great relevance in the present grain growth and densification estimations owing to the small grain size of about 80 nm of the nearly elementary grains (see Figure 1a), showing low degree of agglomeration. As a final characteristic and considering

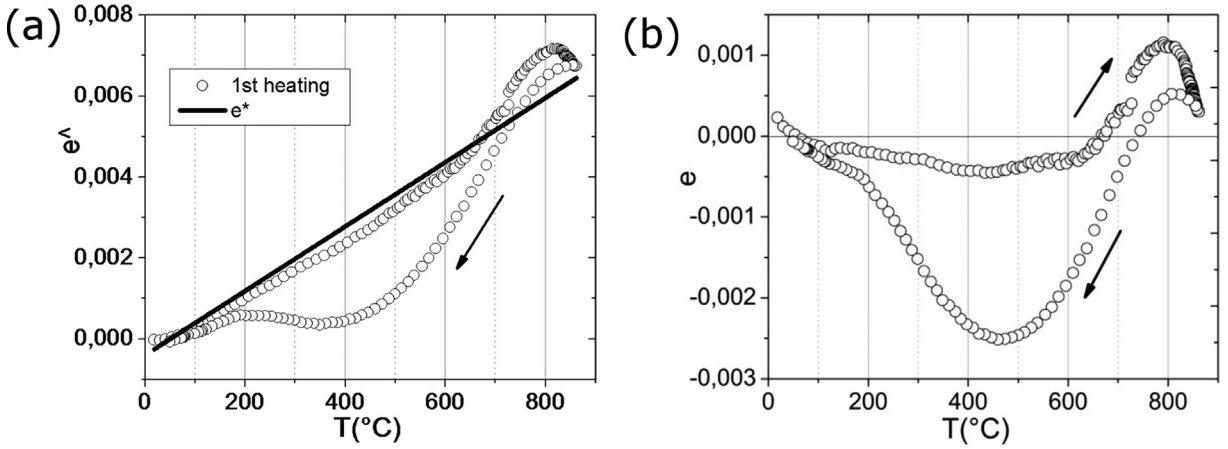

Fig. 7. (a) Expansion of specimen M8 after 1st heating (M8a); (b) Estimation of residual stresses based on data in Figure 7a.

DOI: 10.1002/adem.201600544

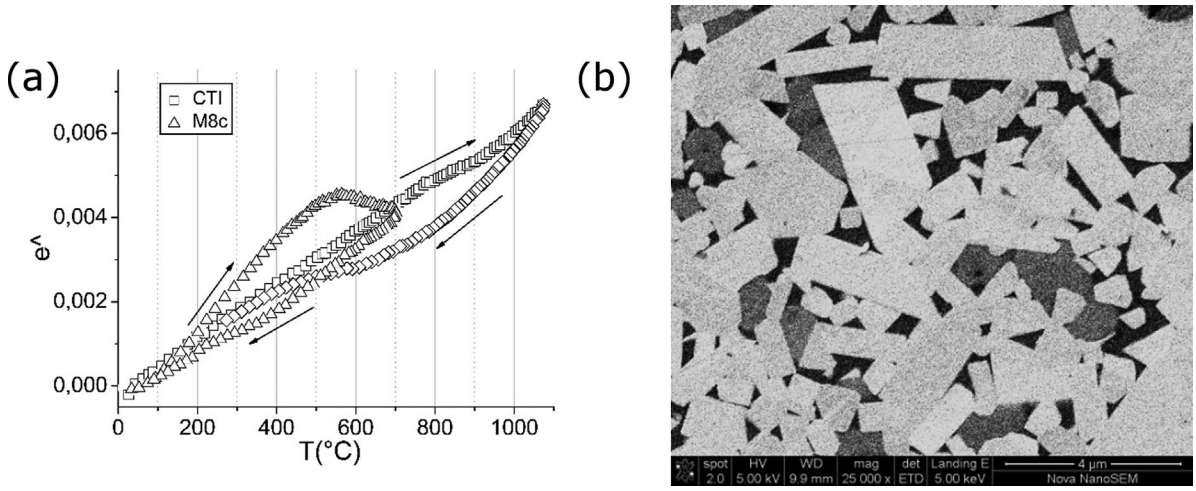

Fig. 8. (a) Thermal cyclings for specimens M8c and commercial WC–TiC–Co sample; (b) Microstructure of WC–TiC–CoCTI specimen.

the present grain sizes distribution, no exaggerated grain growth for fully sintered specimens (Figure 2) was detected. That could be due to a kind of Zener pinning by surface contamination of WC-pure by oxide, subcarbide, some carbon layers or by the second phase cobalt deposited on the surfaces of the elementary grains. By maintaining a small grain size an appreciable densification driving-force can be kept acting during densification. Furthermore, the synthesis step in this work concerning long and soft milling action provided by lengthy stirring-mixing (24 h) and a reasonably small size of Co particles (see Figure 1b) is relevant in producing a "very homogeneous distribution of Co" within the WC-grains and a system of de-agglomerated WC-particles due to the soft milling action of the WC grains on themselves.

It was decided to study WC-Co composites with 20 wt% Co to compare the formation of crystal phases in the system WC-Co with that for WC-Fe composites formed by sol-gel.[11] To study the phases WC, Fe, and subcarbides Fe_3W_3C/Fe_6W_6C, as well as the WC/Fe interfaces formed during the in-situ precipitation of both WC and Fe in the nearly amorphous matrices, it was convenient to have compositions with high iron contents. The present XRD analysis, including Rietveld fittings, as well as the dilatometric cyclings, were carried out on these 20wt% Co samples having no extra carbon added; some of them also contained ultrafine colloidal alumina.

Concerning the crystal phases and microstructure of specimens with 20 wt% Co having additions of ultrafine alumina, and no extra carbon added (MxA samples), it was found that such formulations were apt to produce nearly pure WC/Co hard metals. The addition of alumina nanoparticles can be also useful to add hardness to these materials. Furthermore, the microstructure of sintered MxA compositions were very similar to that for the undoped Mx compositions (compare Figure 2c and d). This may suggest that good densification can be obtained for the present MxA compositions. However, no "reduced grain size" was detected for this system, suggesting that after the present experimental conditions, Al_2O_3 "is not acting" as a grain growth inhibitor. This statement is indeed valid for alumina "agglomerates" rather than for well dispersed alumina particles of about 6 nm. TEM data about eventual distribution of such ultra fine particles on the surfaces of WC elementary grains is not yet available.

For M1/M1A, M2/M2A, M5/M5A, M6/M6A, and M8 (particularly for the machined (and polished) or bulk M8) globally was detected an "expansion" of the hexagonal unit cell, which could be explained by these pellets having internal stresses such as the WC grains are subjected to net "tensile" stresses at RT.

For some of these compositions, having or not additions of ultrafine alumina, materials having either pure WC and Co phases or having some small quantities of subcarbides precipitated (as well as the principal WC and Co phases) were obtained. No clear sintering step could be found to explain the occasional presence of such subcarbides. Although, such finding could be probably associated to some uncontrolled inlet of minor levels of oxygen from the surrounding atmosphere, reducing the carbon to substoichiometric levels.

As described before these 20 wt% Co samples showed a slightly expanded WC-unit cell. Furthermore, it has been verified by XRD-measurements using samples after gradual machining (and polishing) that the above effect of expansion of the WC-unit cell remained valid also within the "bulk" of the pellets. Whether this behavior can be related or not to: i) the sintering protocol, or ii) some WC-doping effects like with Co or eventual impurities, or iii) related to particular behaviors of the final 20%Co pellet-specimens like internal differential strains, or iv) including particular heterogeneous volumetric distribution of the liquid phase in the final composites ref.;[26] pages 97–99, remains somehow unclear. However, there could be important support to this effect being caused by the presence of differential residual stresses evidenced by the hysteretic elastoplastic thermal expansion nature and perhaps anisotropic (in-plane versus perpendicular directions) expansion behavior, in the thin pellet specimen, presented earlier (Figure 5a and b) and discussed next.

ADVANCED ENGINEERING MATERIALS **2017**,
DOI: 10.1002/adem.201600544

As noted above, the overall in-plane expansion-cycle in Figure 5a (and in Figure 7a and b) corresponding to the in-plane "first" heating cycle (M8a; open circle symbols) indicates that the sample initially expands roughly as expected for a composite WC/Co having ≈30%v/v Co second phase. At roughly 600 °C the expansion increases at Co-rate probably due to enough softening of such Co binder and consequently not accepting stress/strain- transfer from the composite-matrix and start expanding at Co-rate till roughly 830 °C, where the cobalt probably starts losing connectivity, permitting WC-WC direct contacts provoking, in turn, a clear decrease in overall expansion of the diphasic composite. As specimen M8a cools from 860 to 450 °C, it contracts roughly at Co-rate and for $T \leq 200$ °C the contraction continues again at the lower composite rate. Now, the overall strain difference $e(T) = e\hat{}(T) - e^*(T)$ (modelled as a net strain acting on the composite) shows positive values up to about 80 °C and then it becomes negative (as expected) and remains roughly constant up to 600 °C. At 670°C, it becomes positive again, up to about 800 °C, owing to probably the free expansion of Co. Examining the 3rd heating in-plane in Figure 5a and 6a, the specimen M8c expands at composite-rate only up to 200 °C, and then at a higher rate up to about 500 °C, at which point the specimen contracts slightly up to the end (700 °C) of this run. On cooling, the specimen contracts at roughly the composite-rate down to 400 °C. The $e = e\hat{} - e^*$ values are still positive around RT, meaning within the present approximations (e^*, e^), that the composite at RT is still under the action of tensile stresses. Indeed and as presented in section 2.2 for the M8 sample a slightly expanded WC unit cell was also measured. Again it is to remark that the matrix would be the WC-grain network and the second phase is provided by the 30%v/v Co added. By considering Figure 6b and 7b it is also apparent some relaxation in the strains is occurring with increasing the number of cycles. Each subsequent-cycle-sample expanded initially with a coefficient close to 75×10^{-7} $(1/T(°C))$ up to 600 °C (1st heating cycle), 300 °C (2nd cycle), and 200 °C (3rd cycle), and then, the specimens continued to expand exhibiting a higher expansion coefficient close to that for Co. Furthermore, at about 815 °C (1st cycle), 740 °C (2nd cycle) and 525 °C (3rd cycle) the expansion coefficient decreased to WC-expansion values. These changes are apparently consistent with a system exhibiting strong relaxation upon further heating/cooling cycles. It could be attributed to reorganization/redistribution of stresses in the Co phase and perhaps to the residual porosity. That is, from the modelled strains estimation by Masutti,[24,25] using the long fibre/polymer matrix (having good adhesion between fibres and matrix) configuration. It can be suggested from data in Figures 6b and 7b that some "tensile" strains may be acting in these composites a temperatures close to RT, which can explain the WC-unit cell expansion as measured by XRD.

It is interesting to note that in ref.[27] residual stress determinations from neutron scattering data of WC – 11 wt% Co specimens are presented. The *a*- and *c*- unit cell parameters of WC were plotted as a function of temperature in the range RT–1 027 °C. As expected, the stresses during heating up are compressive from RT up till 1 027 °C, exhibiting an increase in absolute strain at about 447 °C. However, upon cooling from 1 027 °C the stresses become tensile at ≈920 °C and remain tensile till 547 °C, when they go into compressive again and remain in that state till RT. In the present monolithic samples, and using the rough net strain $e = e\hat{}$-e^* estimation (Figure 7b), it is noted that on heating initially (M8a) the strains are tensile up to 80 °C and then they become compressive till around 650 °C. Between 650 and 850 °C the strains are tensile and remain so upon cooling down to 750 °C where the strains change from tensile to compressive again; they remain so till 30–50 °C.

So far, the data in Figure 5b about the greater relative expansion along the perpendicular direction, as compared to that for the in-plane direction, might be considered as responsible for the suggested small tensile stress acting on these as-made thin pellets. As for the reasons explaining such anisotropic expansion behavior, it could be considered a kind of delamination effect, provoking somehow a weaker composite in the perpendicular direction. Furthermore, such effect could be associated to the rather high 30 v/v% level of Co in these thin composites. However, no extra measurements could be effected yet to check such eventual defects.

Similar measurements on probably very differently made samples of WC + TiC − Co gave similar hysteresis loops as for the present WC + 20wt% Co specimens. Particularly a "softening" temperature at around 800 °C is observed indicating probably that the Co phase reached a soft-state and the composite stopped its expansion. Such data could support the present residual stresses-analysis of these WC + 20% Co samples.

4. Conclusions

Reasonable explanations for the X-rays measured expansion of the WC unit cell in the analyzed sample could be found by independently measured dilatometric thermal expansion cyclings.

That is, after modeling the data, both the in-plane and perpendicular associated expansivity loops-data seem to agree with the above simple model suggesting tensile forces acting on the WC phase at room temperature. However, after heating to about 50–80 °C (depending on the cycle runs) the strains/stresses become clearly compressive as expected for WC–20% Co composites.

Article first published online: xxxx
Manuscript Revised: November 22, 2016
Manuscript Received: August 2, 2016

[1] S. K. Sahay, S. B. Kumar, B. Goswami, A. K. Ray, *J. Metall. Mat. Sci.* **2007**, *49*, 143.

[2] Z. Zak Fang, X. Wang, T. Ryu, K. S. Hwang, H. Y. Song, *Int. J. Refract. Met. Hard Mater.* **2009**, *27*, 288.
[3] F. F. P. Medeiros, S. A. de Oliveira, C. P. de Souza, A. G. P. da Silva, U. U. Gomes, J. F. de Souza, *Mater. Sci. Eng. A* **2001**, *315*, 58.
[4] R. P. Herber, W. D. Schubert, Benno Lux, *Int. J. Refract. Met. Hard Mater.* **2006**, *24*, 360.
[5] C. Barbatti, J. García, P. Brito, A. Pyzalla, *Int. J. Refract. Met. Hard Mater.* **2009**, *27*, 768.
[6] T. W. Penrice, *J. Mater. Shaping Technol*. **1987**, *5*, 35.
[7] L. Prakash, in *Proc. 13th Plansee Seminar*, Vol. 2 (Eds: H. Bildstein, R. Eck), Metallwerk Plansee, Reutte, Austria **1993**, p. 80–109.
[8] C. Hanyaloglu, B. Aksakal, J. D. Bolton, *Mater. Charact*. **2001**, *47*, 315.
[9] W. H. Jiang, J. Fei, X. L. Han, *J. Mat. Sci. Lett*. **2001**, *20*, 283.
[10] C. J. R. G. Oliver, A. Caneiro, J. García, *Procedia Mater. Sci*. **2012**, *1*, 95.
[11] E. A. Álvarez, J. García, E. R. Benavídez, C. J. R. G. Oliver, *Adv. Eng. Mater.* **2015**, *17*, 148.
[12] L. Froschauer, E. M. Fulrath, *J. Mater. Sci*. **1976**, *11*, 142.
[13] G. S. Upadhyaya, S. K. Bhaumik, *Mater. Sci. Eng. A* **1988**, *105/106*, 249.
[14] L. Åkesson, *Thermochim. Acta* **1979**, *29*, 327.
[15] D. Demirskyi, A. Ragulya, D. Agrawal, *Ceram. Int*. **2011**, *37*, 505.
[16] J. García, W. Lengauer, *Mikrochim. Acta* **2001**, *136*, 83.
[17] M. Omori, *Mater. Sci. Eng. A* **2000**, *287*, 183.
[18] C. J. R. G. Oliver, E. A. Álvarez, J. L. García, *Int. J. Refract. Met. Hard Mater.* **2016**, *59*, 121.
[19] http://imagej.nih.gov/ij/
[20] S. Lay, C. H. Allibert, M. Cristensen, G. Wahnström, *Mater. Sci. Eng. A* **2008**, *486*, 253.
[21] A. D. Krawitz, D. G. Reichel, R. Hitterman, *J. Am. Ceram. Soc*. **1989**, *72*, 515.
[22] P. Hidnert, J. *Res. National Bur. Stand*. **1937**, *18*, 47.
[23] C. Larsson, M. Odén, *Int. J. Refract. Met. Hard Mater.* **2004**, *22*, 177.
[24] D. Masutti, J. P. Lentz, F. Delannay, *J. Mater. Sci. Lett*. **1990**, *9*, 340.
[25] H. E. Nassini, M. Moreno, C. G. Oliver, *J. Mater. Sci*. **2001**, *36*, 2759.
[26] D. Hull, *An Introduction to Composite Materials*, Syndicate of the University of Cambridge, The Pitt Building, Trumpington Street, Cambridge, CB2 1RP, Great Britain **1981**, p. 97.
[27] D. Mari, A. D. Krawitz, J. W. Richardson, W. Benoit, *Mater. Sci. Eng. A* **1996**, *209*, 197.

ADVANCED ENGINEERING MATERIALS **2017**,
DOI: 10.1002/adem.201600544